

An IIW residual stress profile estimation scheme for girth welds in pressure vessel and piping components

Pingsha Dong¹ · Shaopin Song¹ · Xianjun Pei¹

Received: 12 January 2015 / Accepted: 18 December 2015 / Published online: 4 February 2016
© International Institute of Welding 2016

Abstract Over the years, one major objective of IIW Joint Working Group (JWG) on residual stresses and distortion prediction (RSDP) has been the development of consistent residual stress profiles for supporting fitness-for-service assessment of welded components. As a result of the JWG activities and further in-depth investigations, this paper presents a major development on a novel full-field residual stress estimation scheme that can be used for describing through-thickness residual stress profiles not only within a weld region, but also at any location away from a weld in pressure vessel and piping components. Within weld region, a systematic parametric finite element analysis is used to establish key parameters that govern through-thickness residual stress distribution characteristics by introducing membrane, bending, and self-equilibrating based decomposition technique. Away from weld region, a shell theory based method is developed for describing through-thickness residual stress distribution at any distance away from weld toe. This paper presents detailed results for single “V” joint preparation with pipe wall thickness varying from 6.25 to 250 mm and wall thickness to pipe radius ratio (r/t) varying from 2 to 100. The residual stress estimation method can be applied for double V and narrow groove joint preparations for girth welded components

since all three joint preparations have been shown to follow a similar functional form to that seen in single V joint preparation.

Keywords (IIW Thesaurus) Residual stresses · Circumferential welds · Fitness-for-service · Stress distribution · Finite element analysis · Pressure vessels · Tubes and pipes

1 Introduction

International Institute of Welding (IIW) Commission X on Fracture Avoidance formed a Joint Working Group (JWG) on residual stress and distortion prediction (RSDP) with Commission XIII on Fatigue of Welded Structures and Commission XV on Design of Welded Structures some years ago. In addition to performing a detailed Round Robin on residual stress modeling techniques available at the time (see Dong and Hong [1]), one of the main objectives of this JWG has been the development of more consistent residual stress profiles than those prescribed in some of the widely-adopted structural integrity assessments, e.g., BS 7910:2013 [2], R6 [3], API 579 RP-1/ASME FFS-1 [4], among others.

Prescribed residual stress profiles in these procedures are intended to provide upper-bound residual stress prescriptions based on available finite element analyses and experimental measurements at weld locations such as weld centerline and weld toe positions. It is known that these prescribed residual stress profiles can exhibit a significant variation from one procedure to another for a given weld configuration with identical welding conditions, as demonstrated by Bouchard [5], by Dong and Hong [6], and most recently by Dong et al. [7]. Moreover, needs often arise for describing residual stress distributions away from weld location, where residual stresses

Recommended for publication by Commission XIII - Fatigue of Welded Components and Structures

✉ Pingsha Dong
dongp@umich.edu

¹ Welded Structures Laboratory, Department of Naval Architecture and Marine Engineering, University of Michigan, Ann Arbor, MI 48109, USA

can be significant, depending upon pipe or vessel geometry, particularly when a through-thickness axial residual stress distribution exhibits a “global bending” type as illustrated by Dong and Hong [6]. At present, guidance for estimating through-thickness residual stress profile as a function of distance away from weld is nearly non-existent in most of the above structural integrity assessment procedures as discussed in [7]. For instance, the 2007 579 RP [4] only provides a single curve based upper-bound estimate of axial and hoop residual stress profiles for locations away from weld toe for all cases of girth welds, even though some recent investigations [6–10] have clearly illustrated that both pipe r/t ratio and heat input, among others, can have a significant impact on through-thickness residual stress distribution characteristics, e.g., either in the form of a rather localized distribution (e.g., of self-equilibrating type) within weld region or a more wide spread distribution (e.g., of global bending type) over a quite distance away from weld. The most recent critical review on residual stress profiles given by some of the FFS codes and standards [2–4] can be found in Dong et al. [7], including detailed comparative assessments between code-stipulated residual stress profiles and validated finite element solutions for a number of selected girth weld configurations.

By building upon numerous investigations performed by participants within IIW JWG on RSDP and research results available in recent literature, this paper presents a novel residual stress profile estimation procedure for girth welds in pressure vessel and piping components. This is accomplished by systematically synthesizing a large amount of residual stress modeling and measurement results so that key contributing parameters that govern important residual stress distribution characteristics over a large spectrum of component geometries and welding parameters can be established. The extraction of these key parameters and understanding of their effects on important residual stress distribution characteristics enable the development of basic functional forms on which residual stress profiles can be established for a broad spectrum of component geometry and welding conditions. Then, a residual stress profile so established should facilitate an introduction of a conservative margin in a consistent manner for achieving a conservative FFS assessment.

This paper starts with a brief description of the finite element based residual stress modeling procedure adopted in this study, which has been validated by various applications [8–15], including work presented at IIW JWG on RSDP over the years, e.g., [1]. A validation study is presented on a girth weld geometry that is of direct relevance to this investigation. A comprehensive parametric study on girth welds is then summarized to demonstrate how key controlling parameters are extracted and defined for supporting the development of a consistent residual stress profile estimation scheme within weld area. A shell

theory based model is formulated for providing an effective means for estimating residual stress profiles beyond weld region until residual stresses completely vanish.

2 Modeling procedure

The finite element residual stress modeling procedure adopted here has been validated and documented in a number of earlier publications [10–16]. The modeling procedure can be characterized as a sequentially coupled thermo-mechanical analysis using ABAQUS [17], in which temperature history is generated first based on a simplified welding heat flow solution method [11] and then followed by a nonlinear thermo-mechanical analysis. In the latter analysis, a unified weld material constitutive model [16] is used for simulating metal deposition, melting/re-melting and solid state phase transformation effects. Detailed discussions on the theories and numerical procedures can be found in the aforementioned references and are not repeated here due to space limitation. Instead, only relevant numerical considerations to this study are demonstrated through an example on which experimental measurements are recently available for facilitating the discussions of parametric analysis results in later sections.

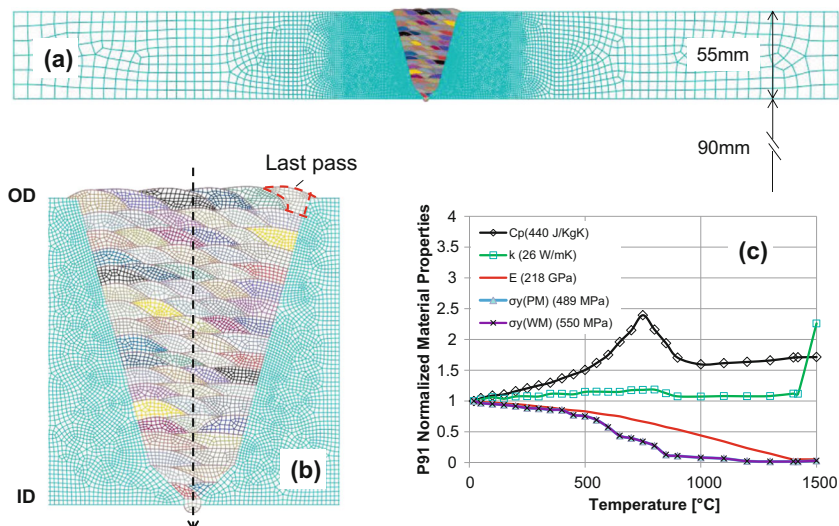
2.1 A case study

The details of a P91 pipe girth weld geometry and weld cross-section are available in [18, 19]. The mock-up weld was made with a single V preparation and 73 weld passes. Residual stresses were measured using X-ray diffraction at the girth weld outer surface (or OD) and a deep-hole drilling (DHD) technique through wall thickness along weld centerline. The measured data used here for validation purpose are directly taken from [18].

An axisymmetric finite element model with 14,893 nodes and 14,662 quadrilateral linear elements is created for this case, as shown in Fig. 1. Detailed weld pass profiles (see Fig. 1b) are modeled according to the descriptions given in [18], and temperature-dependent material properties corresponding to P91 are directly taken from [18] as shown in Fig. 1c. Note that all material properties are normalized by their respective values at ambient temperature 20 °C. The stress-strain curves for both base material and weld metal are assumed to follow the same hardening behavior beyond their respective yield strengths. Von Mises yield criterion following isotropic hardening law (see [11, 20] for detailed justifications) is adopted for both this case study and all parametric analyses reported in this paper.

In performing welding heat flow analysis, heat input for each pass is simulated by assuming a deposition temperature of slightly above material melting temperature

Fig. 1 A mock-up girth weld. **a** Axisymmetric model. **b** Weld pass details modeled. **c** Temperature-dependent properties [18]



1420 °C, i.e., 1650 °C in the present study, consistent with procedures in number of earlier publications [11, 12]. At and above melting temperature, all the material properties are assumed to be constant except the thermal conductivity which is assumed to be doubled in order to account for the enhanced convection associated with molten weld pool. In the thermo-mechanical analysis, time-dependent temperature distributions obtained in the thermal analysis are treated as temperature history input to thermo-mechanical analysis for computing thermal stress history until room temperature is attained, resulting in final residual stress state. Boundary conditions are imposed in such a way that eliminates all rigid body motions without over constraint. This is achieved by simply restraint axial displacement at one end of the pipe wall in this axisymmetric model. Plastic strain annealing temperature sets at 1200 °C for all cases in the unified weld material model, see details in [16].

Effects of solid state phase transformation on residual stresses are taken into consideration because of P91 steel’s hardenability. As given in [19], the starting temperature for martensitic transformation is estimated at 375 °C and finishing temperature at 185 °C. The Koistinen-Marburger relationship is employed to describe the transformation effect. In order to account for the volumetric change associated with a full martensitic transformation, a strain value is chosen as 3.75×10^{-3} [19]. The austenitic transformation temperature is from 820 to 920 °C [19]. The strain due to volumetric change in a full austenitic transformation is -2.288×10^{-3} [19]. As far as residual stresses are concerned, the austenitic transformation is less significant compared with the martensitic transformation in this study. This is mainly owing to the fact that the austenitic transformation occurs at a rather high temperature at which stresses are very small, almost negligible. In

the unified weld constitutive model, thermal strain and phase transformation strain (based on empirical equations in [19]) are superimposed in an incremental formulation to allow two separate paths for heating and cooling.

2.2 Modeling results

Through-thickness residual stress distributions are compared between deep-hole drilling (DHD) measurement [18] and the finite element analysis (FEA) results along weld centerline in Fig. 2. It can be seen that modeling results and residual stress measurements show an overall good agreement. The discrepancies near OD surface may be attributed to the following considerations: (1) phase transformation effects in this case are found contributing significantly to the very localized

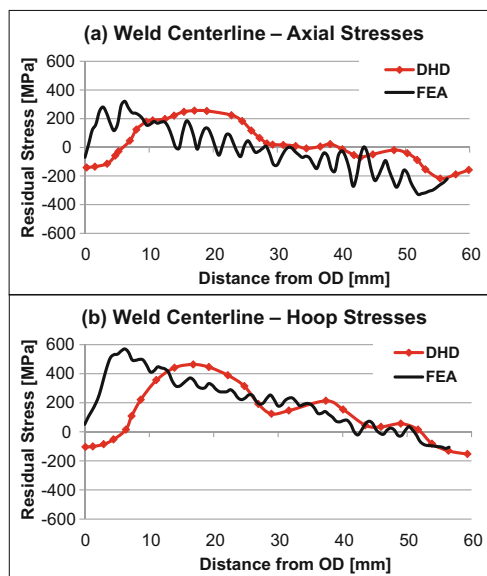


Fig. 2 FE results versus deep-hole drilling (DHD) measurement data along weld centerline. **a** Axial stresses and **b** hoop stresses

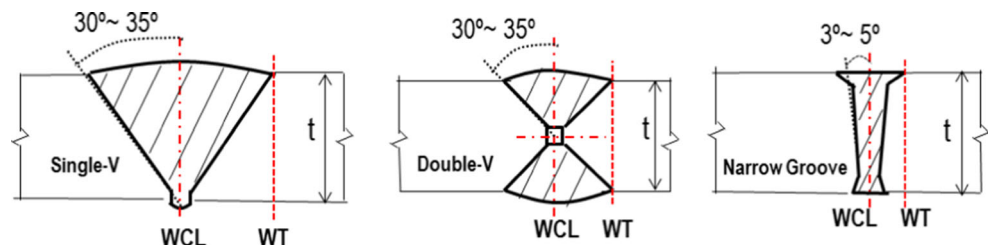
residual stress features shown in Fig. 2, which are associated with actual weld pass geometries and positions, while the model (see Fig. 1b) only represents an idealized layout of weld passes; (2) the original authors [18] reported that the validity of the DHD measurements in through thickness direction was deemed questionable within a depth of 12 mm from OD surface, suggesting that the measurement data should be considered valid from a depth beyond 12 mm from OD surface up to 48 mm. With this in mind, the FEA results from this study show a rather good agreement with the measurements for both residual stress components.

3 Key parameter identification through parametric analysis

A large number of parametric residual stress analyses for pipe/vessel girth welds have been performed by varying pass size, welding sequence, radius to wall thickness ratio (r/t), thickness (t), joint preparation, material, as well as heat input. In dealing with hundreds of cases and associated residual stress distributions, an effective data reduction technique is essential. Such a technique should allow the extraction of important residual stress distribution features that are deemed important to fracture mechanics based defect assessment while retaining their mechanics underpinnings. The latter is necessary for developing simplified but mechanistically sound residual profile prescriptions. Owing to the nature of well-defined restraint conditions such as in the radial direction in girth welds, the length-scale based residual stress decomposition procedure discussed by Dong [8] is adopted in this study. For any given residual stress distribution $\sigma(x)$, where x is measured from pipe inner surface (ID), its statically equivalent through-thickness membrane (σ_m), bending (σ_b), and self-equilibrating ($\sigma_{s.e}$) can be written as:

$$\begin{aligned}\sigma_m &= \frac{1}{t} \int_0^t \sigma(x) dx \\ \sigma_b &= \frac{6}{t^2} \int_0^t \sigma(x) \left(\frac{t}{2} - x\right) dx \\ \sigma_{s.e.} &= \sigma(x) - \sigma_m - \sigma_b \left(1 - \frac{2x}{t}\right)\end{aligned}\quad (1)$$

Fig. 3 Representative joint preparations investigated in this study. Single V (SV), double V (DV), and narrow groove (NG)



where t is pipe wall thickness. It has been demonstrated by Dong [8] and Dong and Hong [11] that membrane part σ_m and bending part σ_b play a key role in contributing to fracture driving force in fracture assessment while the contribution of $\sigma_{s.e}$ part is only limited to when a crack is rather small (i.e., up to a crack size of 0.1~0.2 t). Beyond this small crack size, stress intensity factor due to the self-equilibrating part starts to decrease and becomes negligible at a crack size of about 0.4 t, as illustrated by Dong [8]. Therefore, Eq. (1) provides a means not only for reducing complex residual stress distributions into simple forms in terms of its membrane and bending content relative to self-equilibrating, but also for extracting residual stress features that are most critical to fracture assessment.

It should be noted that previous studies [5, 6, 21, 22] were focused upon pipe wall thickness less than 50 mm (2"), mostly for single V joint preparation. This study considers a full range of thicknesses varying from 6.35 mm (1/4") to 254 mm (10") with joint preparations of SV, DV, and NG (see Fig. 3), for which a detailed parametric analysis is presented for a large number of SV joint preparation cases while the results for joint preparations involving DV and NG will be discussed for comparison with SV cases for demonstrating similarities and differences. Component base material considered in this parametric study is 2.25CrMo-V type. Figure 4 shows its temperature-dependent properties normalized with respect to their room temperature values at 23 °C. Further details can be found in a two-part paper series by the same authors [23, 24].

3.1 r/t ratio effect

As reported by Dong and Hong [6], Dong [9] and Song et al. [23], component geometry such as r/t ratio can have a significant effect on through-thickness residual stress distribution characteristics. This can be illustrated by considering a series of thick section (100 mm or 4") girth welds as r/t ratio varies, as shown in Fig. 5. Both axial (Fig. 5a) and hoop residual stress components (Fig. 5b) show a continuous change in distribution characteristics as r/t ratio increases from 2 to 100. Specifically, the axial residual stress component at $r/t=2$ clearly exhibits a through-thickness bending dominated distribution, i.e., with outer surface (OD) under tension and inner surface (or ID) under compression. As r/t ratio

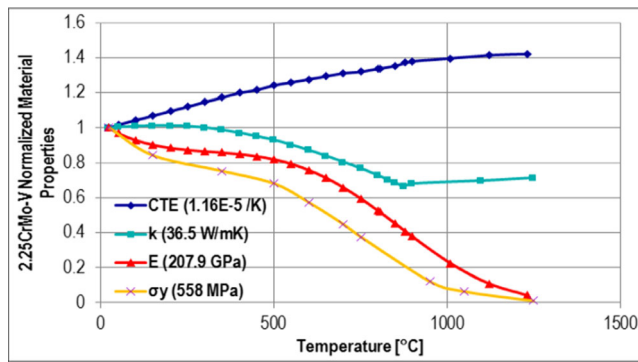


Fig. 4 Temperature dependent material properties for 2.25CrMo-V steel

increases, the compressive residual stress at ID gradually decreases and becomes tensile at r/t reaches to 20, approaching to a self-equilibrating dominated through-thickness distribution type at $r/t=100$. Accompanying the change in axial residual stress distribution, hoop residual stress distribution can be characterized by re-distributing its two compressive zones with respect to the yield-magnitude tensile zone, becoming increasingly aligned in the axial direction.

To quantitatively evaluate r/t ratio effects, the residual stress results shown in Fig. 5 are decomposed into through-thickness membrane and bending parts (normalized by material yield strength) according to Eq. (1) at weld centerline, as shown in Fig. 6. Parametric analysis results for DV and NG joint preparations (see Fig. 3) are also plotted in Fig. 6 for comparison purposes. It can be seen axial bending stress decreases with an increasing r/t ratio (Fig. 6a), following essentially a logarithmic delay as r/t increases, as the curve fitting results suggest. This can be related to the saturation in hoop membrane stress when r/t becomes large, as shown in Fig. 6b. This is accompanied with a rapidly decreasing hoop bending (Fig. 6c). It can be further observed that as far as axial bending stresses are concerned, both SV and NG share a similar magnitude with NG joint preparation giving a

slightly higher value. This can be related to a slightly higher radial restraint by pipe section with a smaller linear heat input in NG joints. The benefits in using DV joint preparation can be clearly seen (Fig. 6a and 6c) as a result of pass deposition sequence that is closer to symmetric conditions with respect to mid-wall surface than other two joint preparations. Residual stresses at weld toe position follow a similar trend and will not be presented here due to space limitation. It should be pointed out that the trends shown in Fig. 6 are consistent with some of the previous findings discussed in [9, 11] in which only a few selected cases on the three joint configurations were investigated, including a recent study by Song et al. [23].

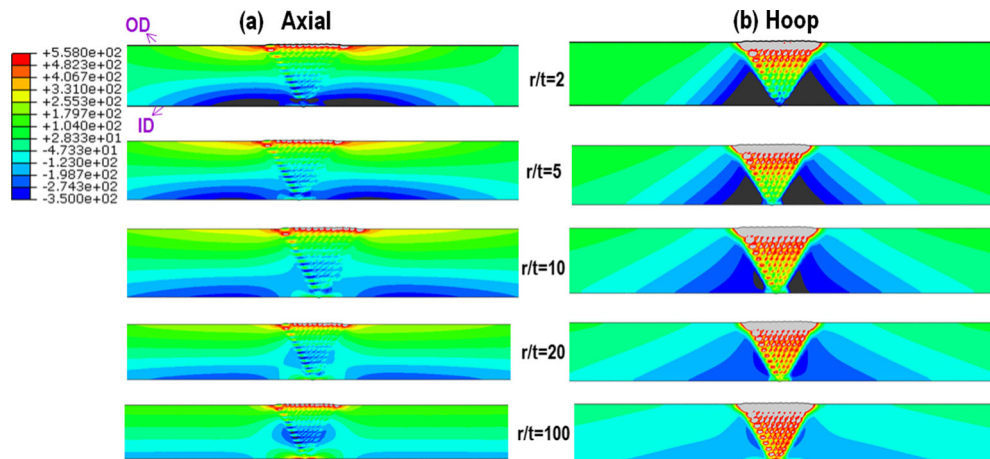
3.2 Heat input effect and parameter formulation

Welding heat input is typically defined as a linear heat input in practice as,

$$Q = \frac{U \cdot I \cdot \eta}{v}, \quad [J/mm] \quad (2)$$

where U is arc voltage, I welding current, η welding efficiency, and v welding travel speed. As discussed in Dong and Hong [11], a relationship between the heat input implied in 2D cross-section models (e.g., axisymmetric or generalized plane strain models) and linear heat input (Eq. 2) used in practice must be carefully established since any 2D heat transfer models cannot directly take into account of heat loss in the third direction, among other things. As a part of this investigation, an analytical-based heat input estimation scheme is introduced for calculating heat input implied in a 2D cross-section model, which can then be related to the conventional linear heat input definition described in Eq. (2). The details of this development and its extensive validations can be found in a separate publication [25]. In what follows, only the relevant results

Fig. 5 Residual stress contour plots for SV girth welds with $t = 100$ mm (4"): r/t ratio effects. **a** axial residual stress and **b** hoop residual stress



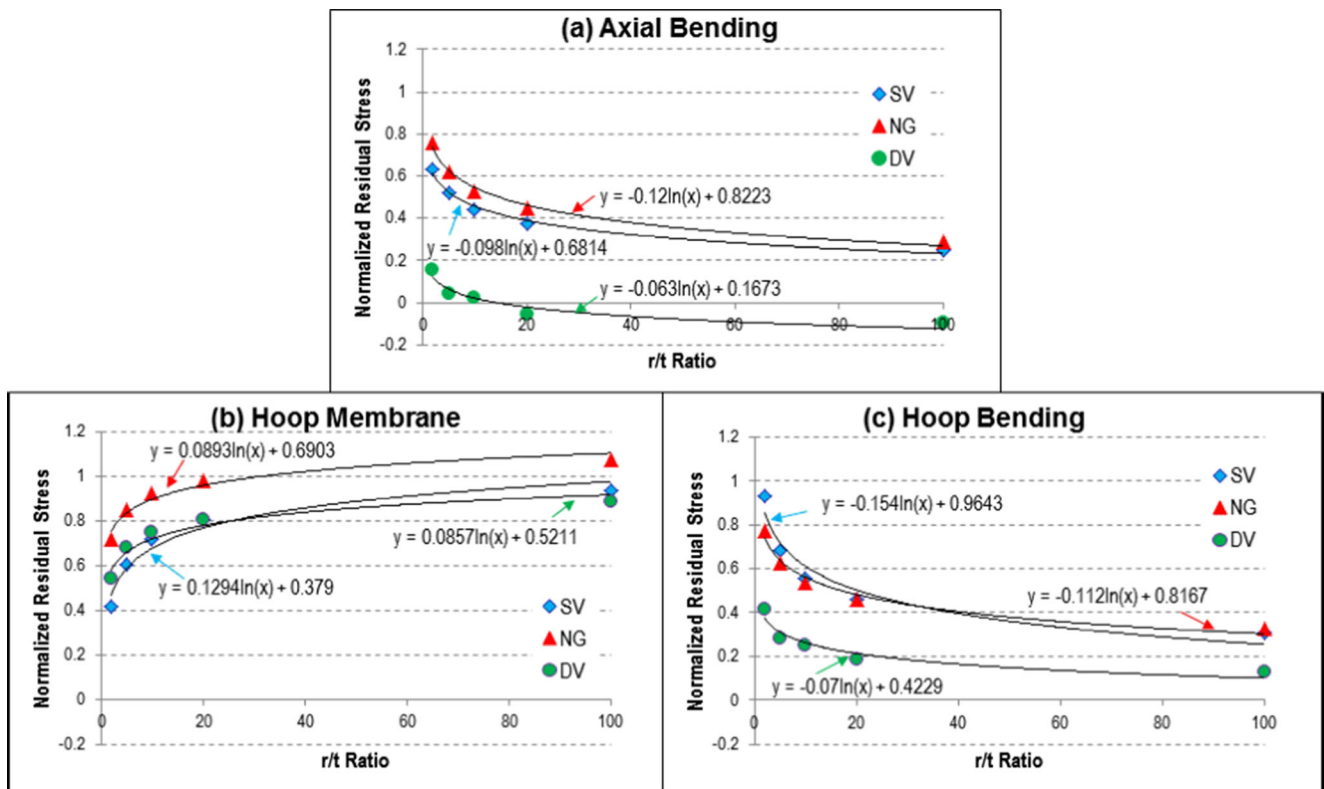


Fig. 6 Comparison of decomposed residual stresses at weld centerline as a function of r/t ratio over three types of joint preparations (SV, DV, and NG). **a** Axial bending stresses, **b** hoop membrane stresses, and **c** hoop bending stresses

are described in support of the present discussions.

In a 2D cross-section welding heat transfer model, a simplified residual stress procedure adopted by various researchers [6–15, 18, 19, 21, 22] involves the following: (1) deposit a molten weld pass at a specified melting temperature; (2) hold the melting temperature for a short period of time (t_{hold}) while transient conduction into its surrounding takes place. The resulting heat input can be separated into two parts:

$$Q_1' = \rho \cdot C_p \cdot \Delta T \cdot A_{pass} \quad , \quad [J/mm] \quad (3)$$

$$Q_2' = 2k \cdot \Delta T \cdot \sqrt{\frac{t_{hold}}{\pi\alpha}} \cdot L_s \quad , \quad [J/mm] \quad (4)$$

In Eqs. (3) and (4), A_{pass} is the averaged cross section area of weld pass deposit represented in a 2D model, ΔT temperature difference between melting and ambient temperatures, L_s weld pass fusion line in contact with the surroundings. In Eq. (3), Q_1' represents an estimate of heat content involved in bringing a weld deposit with a cross-sectional area of A_{pass} per unit length in the welding direction to its melting temperature from initial ambient temperature. In Eq. (4), Q_2' represents the amount of heat that needs to be supplied to FE model for maintaining melting temperature of the weld deposit while transient heat conduction loss into the surrounding material takes

place during a hold time t_{hold} which is approximated with a 1D transient heat conduction model [25].

The total linear heat input represented by a 2D cross-section welding heat transfer model then becomes the sum of the two parts described in Eqs. (3) and (4), i.e.,

$$Q' = (Q_1' + Q_2') \cdot \eta' \quad , \quad [J/mm] \quad (5)$$

where η' is a factor for taking account of additional 3D heat loss not explicitly considered in the development of Eqs. (3) and (4). After a series of benchmarking evaluations against detailed experimental data (see [25] for details), η' value is found to be 1.35 for consistently estimating linear heat input. With Eq. (5), linear heat input represented in a 2D cross-section model can now be directly related to a linear welding heat input given in Eq. (2) without ambiguity.

Past investigations, e.g., by Bouchard [5] and Dong and Hong [6], indicated that linear heat input parameter in Eq. (2) is not capable of effectively correlating residual stress distributions under different heat input conditions, as further demonstrated by Song et al. [23]. Recognizing the deficiencies of above existing heat input parameters in uniquely correlating through-thickness membrane and bending stress content, Song et al. [23] proposed the following characteristic heat input definition, based on a

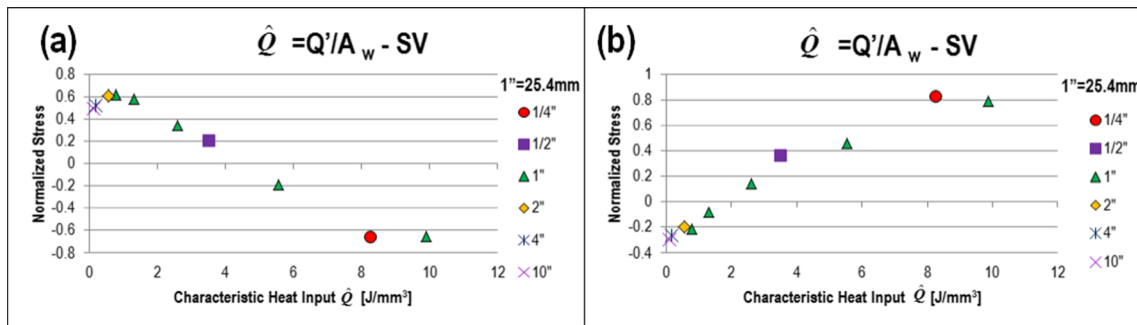


Fig. 7 Decomposed through-thickness residual stresses at weld toe as a function of characteristic heat input \hat{Q} for SV welds ($r/t=10$). **a** Axial bending stresses and **b** hoop membrane stresses

careful examination of a wide range of through-thickness residual stress results obtained in a systematic parameter analysis covering a large span of component geometry, linear heat input, and joint preparation:

$$\hat{Q} = \frac{Q'}{A_w} \text{ (J/mm}^3\text{)} \tag{6}$$

where A_w represents the total fusion zone area in a weldment, corresponding to the area defined by joint preparation profile shown as shaded area in Fig. 3. As such, \hat{Q} represents linear heat input per unit weld fusion zone area.

The effectiveness of the new characteristic heat input parameter described in Eq. (6) is illustrated in Fig. 7 by plotting decomposed residuals stress components as a function of the characteristic heat input \hat{Q} . It is clear that \hat{Q} is indeed effective in correlating both axial and hoop residual stresses for all wall thicknesses investigated. In Fig. 7, hoop membrane stress increases with an increasing characteristic heat input \hat{Q} , implying an increased shrinkage force in hoop direction. As \hat{Q} approaches about 8 J/mm^3 , hoop membrane stresses seem to attain their respective maximum values (at about yield magnitude S_y for SV welds shown in Fig. 7b), causes the strongest axial bending stresses as shown in Fig. 7a (e.g., about 80 % of yield strength level under compression at ID). For NG and DV joint types, the effectiveness of the new characteristic heat input parameter has been demonstrated by Song et al. [23].

4 Residual stress profile estimation scheme—weld region

The two key parameters (r/t ratio and characteristic heat input \hat{Q}) identified from the previous section can be conveniently used for constructing a residual stress profile functional form that is applicable for a wide range of r/t and \hat{Q} . Such a functional form and its solution process are illustrated below.

As implied by the through-thickness residual stress decomposition technique in Eq. (1), any given through-thickness residual stress distribution can be expressed by a combination of three parts, i.e., membrane (σ_m), bending (σ_b), and self-equilibrating ($\sigma_{s.e}$), as:

$$\frac{\sigma(\xi)}{S_y} = \bar{\sigma}_m + \bar{\sigma}_b \xi + \bar{\sigma}_{s.e}(\xi) \tag{7}$$

where ξ is a dimensionless coordinate parameter which is expressed as $\xi=2(x/t)-1$, where x is measured from pipe ID, and S_y is material yield strength. Note that all barred stress components on the right side of Eq. (7) are dimensionless. As demonstrated in earlier sections, both membrane and bending parts are dominated by the two key parameters: component geometry parameter (r/t) and characteristic heat input \hat{Q} .

4.1 Self-equilibrating stress

The self-equilibrating part $\sigma_{s.e}$ is a higher order term and shown to be dominated mostly by joint preparation and weld pass sequence effects among others [8, 11, 20] and can be expressed, for illustration purposes, in a polynomial form, e.g.,:

$$\bar{\sigma}_{s.e}(\xi) = e\xi^2 + f\xi^3 + g\xi^4 + h\xi^5 \tag{8}$$

where the coefficients of $e, f, g,$ and h in Eq. (8) can be directly solved by imposing two self-equilibrating conditions and two consistency conditions at both ID and OD on which surface residual stresses are assumed to be bounded by material yield strength magnitude. The four constants in Eq. (8) can then be expressed as:

$$\begin{aligned} e &= -\frac{3}{4} \left(\bar{S}_+^{s.e.} + \bar{S}_-^{s.e.} \right) \\ f &= -\frac{5}{4} \left(\bar{S}_+^{s.e.} - \bar{S}_-^{s.e.} \right) \\ g &= \frac{5}{4} \left(\bar{S}_+^{s.e.} + \bar{S}_-^{s.e.} \right) \\ h &= \frac{7}{4} \left(\bar{S}_+^{s.e.} - \bar{S}_-^{s.e.} \right) \end{aligned} \tag{9}$$

where $\bar{S}_+^{s.e.}$ is the normalized surface value of self-equilibrating part where bending is positive (tension), and $\bar{S}_-^{s.e.}$ is the normalized surface value where bending is negative (compression). Since both surfaces are undergone yield during welding, $\bar{S}_+^{s.e.}$ and $\bar{S}_-^{s.e.}$ can be defined by introducing a multiplicative factor (K) against material yield strength as follows:

$$\bar{S}_+^{s.e.} = K - \bar{\sigma}_m - |\bar{\sigma}_b| \tag{10}$$

$$\bar{S}_-^{s.e.} = K - \bar{\sigma}_m - |\bar{\sigma}_b| \tag{11}$$

Due to strain hardening and biaxiality effects, normalized peak residual stress may exceed unity. This is accommodated by making K larger than unity, which also serves as a means to achieve a desirable level of conservatism. As an example, API 579 RP [4] assumes $K=1.2$ for axial residual stress and $K=1.5$ for hoop residual stress, respectively.

4.2 Membrane and bending stresses

As illustrated in Section 3, through-thickness membrane and bending stresses can be uniquely related to r/t ratio and characteristic heat input \hat{Q} . By examining the dependency of membrane and bending stresses on r/t ratio as illustrated in Fig. 6, it is found that a logarithmic functional form seems to provide a good description of the variation of the membrane and bending stresses as a function of r/t , e.g.,:

$$\bar{\sigma}_m\left(\frac{r}{t}\right) \text{ or } \bar{\sigma}_b\left(\frac{r}{t}\right) = a \cdot \ln\left(\frac{r}{t}\right) + b \tag{12}$$

where coefficients a and b in Eq. (12) can be related to characteristic heat input \hat{Q} through a curve fitting process.

Therefore, Eq. (12) for membrane or bending stress can be re-written as a function of both r/t and \hat{Q} ,

$$\bar{\sigma}_m\left(\frac{r}{t}, \hat{Q}\right) \text{ or } \bar{\sigma}_b\left(\frac{r}{t}, \hat{Q}\right) = a(\hat{Q}) \cdot \ln\left(\frac{r}{t}\right) + b(\hat{Q}) \tag{13}$$

Thus, the coefficients in Eq. (13) for each of the joint configurations shown in Fig. 3 can be determined through a two-step process described as follows, using hoop membrane stresses at weld toe in SV joints as an example:

- (1) For each given characteristic heat input \hat{Q} value, determine $a_{\theta,m}(\hat{Q})$ and $b_{\theta,m}(\hat{Q})$ values for achieving a best fit of Eq. (13) on r/t dependency;
- (2) Determine $a_{\theta,m}(\hat{Q})$ and $b_{\theta,m}(\hat{Q})$ expressions as a function of \hat{Q} over the range of \hat{Q} values considered in the previous step, as illustrated in Fig. 8 in which a nonlinear least squares method is used.

The results shown in Fig. 8 can be represented by a third-order polynomial function of \hat{Q} as:

$$\begin{aligned} a_{\theta,m}(\hat{Q}) &= 0.0009\hat{Q}^3 - 0.0151\hat{Q}^2 + 0.0801\hat{Q} + 0.0646 \\ b_{\theta,m}(\hat{Q}) &= -0.0019\hat{Q}^3 + 0.022\hat{Q}^2 + 0.0309\hat{Q} - 0.4516 \end{aligned} \tag{14}$$

By following the same procedures described in the above, the coefficients in Eq. (13) for other residual stress components at weld toe in SV joints can be obtained, e.g.,

$$\begin{aligned} a_{\theta,b}(\hat{Q}) &= -0.0008\hat{Q}^3 + 0.0136\hat{Q}^2 - 0.0723\hat{Q} - 0.0785 \\ b_{\theta,b}(\hat{Q}) &= 0.0171\hat{Q}^3 - 0.2085\hat{Q}^2 + 0.6139\hat{Q} + 0.8546 \end{aligned} \tag{15}$$

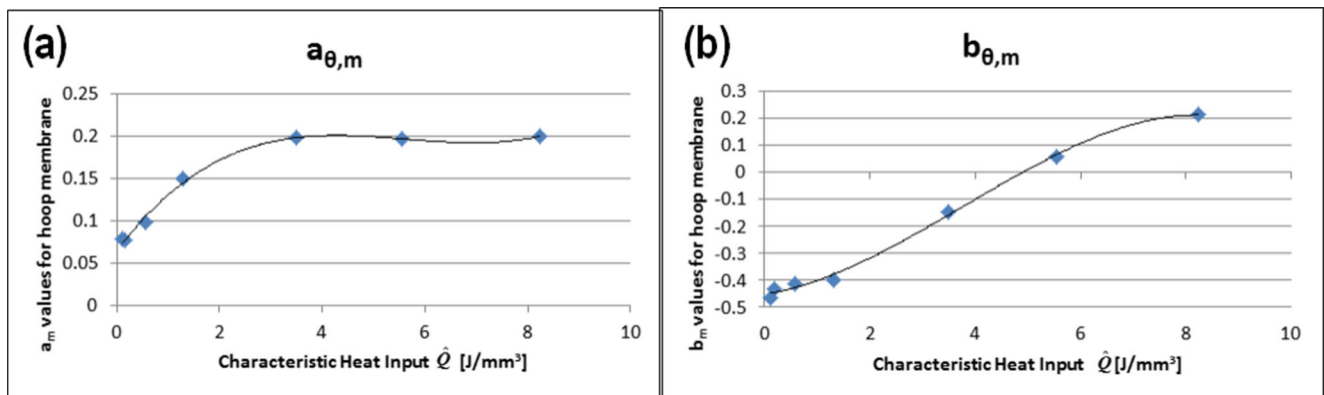


Fig. 8 Curve-fitting results for $a_{\theta,m}$ and $b_{\theta,m}$ for hoop membrane stress at weld toe (SV joints) according to Eq. (13). **a** $a_{\theta,m}$ as a function of \hat{Q} . **b** $b_{\theta,m}$ as a function of \hat{Q}

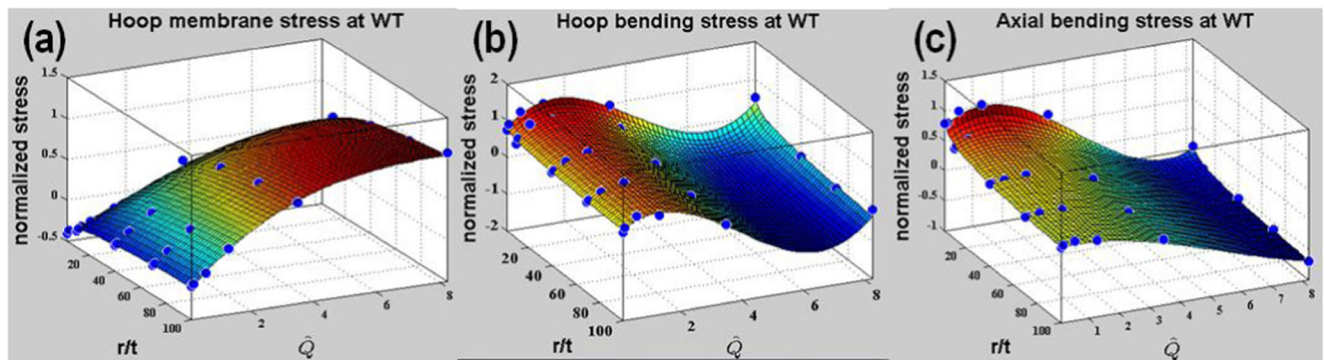


Fig. 9 Comparisons between the proposed estimation method (Eqs. (13)–(16)) and FEA results at weld toe for SV girth welds. **a** Hoop membrane stress according to Eqs. (13) and (14). **b** Hoop bending stress according to Eqs. (13) and (15). **c** Axial bending stress according to Eqs. (13) and (16)

for hoop bending stresses, and

$$\begin{aligned} a_{x,b}(\hat{Q}) &= -0.002\hat{Q}^3 + 0.0258\hat{Q}^2 - 0.0716\hat{Q} - 0.1268 \\ b_{x,b}(\hat{Q}) &= 0.0122\hat{Q}^3 - 0.1631\hat{Q}^2 + 0.3864\hat{Q} + 0.826 \end{aligned} \quad (16)$$

for axial bending stresses.

Three-dimensional plots of membrane and bending stresses based on Eqs. (13)–(16) are shown in Fig. 9 in which the corresponding stress components computed by FEA for selected cases are also shown for comparison purpose. It can be seen that a good agreement is achieved between estimations using Eqs. (13)–(16) and FEA results. The overall correlation coefficient R^2 is above 0.99, and standard deviation is within 0.03. With the same procedure, the membrane and bending stresses for other joint preparations can be generated in the same manner, which will not be reported here due to space limitation.

5 Residual stress profile—outside weld region

As far as residual stresses at some distance away from weld region are concerned, it can be argued that only membrane

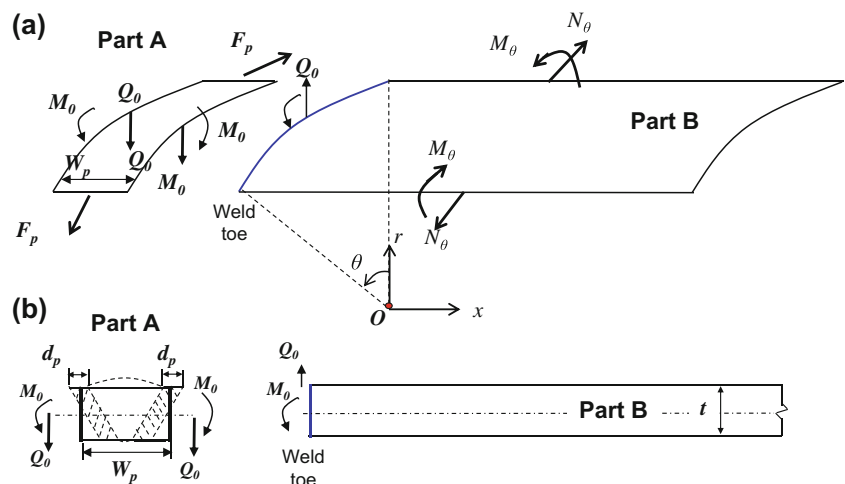
and bending parts are operative while self-equilibrating part remains local to weld area [8, 11, 20]. With such considerations, a classical shell theory based solution should provide a reasonable functional description of through-wall membrane and bending stress distributions under prescribed loading conditions in terms of forces and moments generated by weld zone against the rest of the shell body.

5.1 Formulation

In the context of shell theory, it is assumed that residual stress distribution in a girth-welded cylindrical component can be modeled as an assembly of two shell sections, as shown in Fig. 10. Part A represents an equivalent plastic zone width along the shell mid-thickness while part B represents the rest of the component section. The interactions between the two parts are through a ring shear force Q_0 in radial direction and a ring moment M_0 . The ring force (consistent with line force definition with a unit of, e.g., N/mm) can be related to hoop shrinkage force F_p induced by plastic zone (part A) position on shell mid-thickness, as:

$$Q_0 = \frac{F_p}{2r} = \frac{\sigma_{\theta,m}^{ave} \cdot W_p \cdot t}{2r} \quad (17)$$

Fig. 10 A two-part shell assembly model (Part A: Equivalent plastic zone (W_p) along shell mid-thickness; Part B: Remaining shell section). **a** 3D view. **b** Through-thickness cross-section view



In Eq. (17), W_p represents the equivalent plastic zone width situated on shell mid-surface, as shown in Fig. 10b, in which d_p stands for the depth of plastic zone beyond weld fusion zone and its estimation method is to be given in the next section. The average hoop residual stress $\sigma_{\theta,m}^{ave}$ in Eq. (17) can be approximated by the membrane part of hoop residual stress obtained at weld centerline, which can be obtained through the residual stress profile estimation procedure for weld region as described in Sec. 4. The coefficients in Eq. (13) corresponding to hoop membrane stress at weld centerline in SV joints are given below:

$$\begin{aligned} a_{\theta,m}(\hat{Q}) &= 0.0013\hat{Q}^3 - 0.0172\hat{Q}^2 + 0.0469\hat{Q} + 0.1281 \\ b_{\theta,m}(\hat{Q}) &= -0.0088\hat{Q}^3 + 0.1124\hat{Q}^2 - 0.2724\hat{Q} + 0.3791 \end{aligned} \tag{18}$$

As a result of the shell model idealization shown in Fig. 10b, actual weld toe position in a girth welded component can be assumed, for convenience, to be situated at the interface between part A and part B for facilitating the development of the final assembled solution. Then, the ring moment M_0 (consistent with line moment definition with a unit of, e.g., N-mm/mm) can be directly expressed in terms of bending part of axial residual stresses at weld toe $\sigma_{x,b}^0$ that is already available in Eqs. (13) and (16) as:

$$M_0 = \frac{t^2}{6} \sigma_{x,b}^0 \tag{19}$$

With both ring shear force (Q_0) and ring moment (M_0) being determined as discussed above, both radial deflection and line moment as a functional axial distance x can be analytically expressed through classical shell theory [26], as:

$$w(x) = \frac{1}{2\beta^3 D} [\beta M_0 e^{-\beta x} (\cos\beta x - \sin\beta x) - Q_0 e^{-\beta x} \cos\beta x] \tag{20}$$

$$M_x(x) = M_0 e^{-\beta x} (\cos\beta x + \sin\beta x) + \frac{1}{\beta} Q_0 e^{-\beta x} \sin\beta x \tag{21}$$

where, β and D are defined as:

$$\beta = \frac{\sqrt[4]{3(1-\nu^2)}}{\sqrt{rt}}, D = \frac{Et^3}{12(1-\nu^2)} \tag{22}$$

in which r is radius to shell mid-wall surface, t thickness, E Yong’s modulus and ν Poisson ratio. With $M_x(x)$ and $w(x)$

being given in Eqs. (20) and (21), line moment $M_\theta(x)$ and line force $N_\theta(x)$ in the hoop direction shown in Fig. 10a can be obtained as follows:

$$M_\theta(x) = \nu M_x(x) \tag{23}$$

$$N_\theta(x) = \frac{Et w(x)}{r} \tag{24}$$

Once the plastic zone width on shell mid-surface, i.e., W_p in Eq. (17), is determined, radial displacement (Eq. 20), axial moment (Eq. 21), and hoop moment and force in Eqs. (23)–(24) can be directly calculated.

As shown in Fig. 10, the entire plastic zone contributing to the shrinkage force F_p along the hoop direction consists of both weld fusion zone and additional plastic deformation zone beyond fusion boundary area can be described as:

$$A_p = A_w + 2d_p t \approx W_p t \tag{25}$$

where A_w represents weld fusion area which can be estimated based on a given joint preparation or available weld macrograph. A closed form solution for estimating plastic zone extent d_p measured from weld fusion (see [24, 27–28]) can be obtained. Then, its estimation can be written in a simple form as:

$$d_p = \frac{(r_w + 2\sqrt{\alpha \cdot t_{hold} / \pi}) \cdot \Delta T}{4\Delta T_y} - r_w \tag{26}$$

where r_w represents an equivalent radius of a weld pass deposit and ΔT_y is expressed as $(S_y/E)/\alpha$ in which α is material thermal expansion coefficient. As demonstrated in [24], Eq. (26) can also be expressed in terms of the linear heat input Q' given in Eqs. (3)–(5) as:

$$d_p = \frac{Q'}{4\pi \cdot \rho C_p \cdot r_w \cdot \Delta T_y} - r_w \tag{27}$$

It is worth noting that Eq. (27) indicates that plastic zone depth d_p is linearly proportional to welding linear heat input and depends on material’s thermal-physical (ρ, C_p, K, α_T) and mechanical properties (E, S_y), as one would expect.

5.2 Residual stress solution

With the plastic zone area given in Eq. (25), ring force Q_0 can now be calculated from Eq. (17). Equation (21) can then be used to calculate the resulting axial bending residual stress as a

function of x defined in Fig. 10 measured from weld toe position, as:

$$\sigma_{x,b}(x) = \frac{6M_x(x)}{t^2} \tag{28}$$

Note that the membrane component of axial residual stress is negligible since no axial restraint was considered in Section 3 for all cases.

Hoop residual stresses in the form of through-thickness membrane and bending can be estimated in a similar fashion by using $M_\theta(x)$ and $N_\theta(x)$ given in Eqs. (23)–(24):

$$\sigma_{\theta,b}(x) = \frac{6M_\theta(x)}{t^2} \tag{29}$$

$$\sigma_{\theta,m}(x) = \frac{N_\theta(x)}{t} \tag{30}$$

Strictly speaking, Eqs. (29) and (30) or Eqs. (23) and (24) are only applicable for deformation within elastic regime so that Hooke’s law can be directly used to obtain Eqs. (29) and (30). As discussed in Section 5.1 and shown in Fig. 10b, the region described by plastic deformation depth d_p requires an additional treatment in order to avoid discontinuities in the hoop stress components between weld fusion boundary and elastic regime beyond d_p . This can be accomplished by introducing a linear interpolation procedure between stresses at fusion zone boundary and plastic zone boundary. Then, Eqs. (29) and (30) becomes:

$$\sigma_{\theta,b}(x) = \begin{cases} \left(-\frac{\Delta\sigma_{\theta,b}}{d_p}x + \Delta\sigma_{\theta,b} \right) + \frac{6M_\theta(x)}{t^2}, & 0 \leq x \leq d_p \\ \frac{6M_\theta(x)}{t^2}, & x \geq d_p \end{cases} \tag{31}$$

where, $\Delta\sigma_{\theta,b} = \sigma_{\theta,b}^0 - \left[\frac{6M_\theta(x)}{t^2} \right]_{x=0}$

$$\sigma_{\theta,m}(x) = \begin{cases} \left(-\frac{\Delta\sigma_{\theta,m}}{d_p}x + \Delta\sigma_{\theta,m} \right) + \frac{N_\theta(x)}{t}, & 0 \leq x \leq d_p \\ \frac{N_\theta(x)}{t}, & x \geq d_p \end{cases} \tag{32}$$

where, $\Delta\sigma_{\theta,m} = \sigma_{\theta,m}^0 - \left[\frac{N_\theta(x)}{t} \right]_{x=0}$

In Eqs. (31) and (32), $\sigma_{\theta,m}^0$ and $\sigma_{\theta,b}^0$ are the membrane and bending components of hoop residual stress at weld fusion zone boundary or weld toe, $\Delta\sigma_{\theta,b}$ is the difference between the value obtained from Eq. (29) at $x=0$ and $\sigma_{\theta,b}^0$, and similarly $\Delta\sigma_{\theta,m}$ is the difference between the value obtained from Eq. (30) at $x=0$ and $\sigma_{\theta,m}^0$. Both of $\sigma_{\theta,m}^0$ and $\sigma_{\theta,b}^0$ can be obtained based the estimation procedure developed in Section 4 based on Eqs. (13) and (14) and Eqs. (13) and (15), respectively.

5.3 Analytical versus FE solutions

Consider a girth weld with a thickness of 6.25 mm (1/4”) in single joint V preparation, Figs. 11 and 12 show the results for two cases with r/t ratio of 10 and 100, respectively. The shell theory based estimation results are presented in terms of normalized residual stresses by material yield strength and compared with finite element modeling results over the entire component length starting from weld toe position. The horizontal axis represents distance from weld toe and is normalized by \sqrt{rt} which serves as a characteristic length parameter measuring pipe’s flexibility, as demonstrated for characterizing girth weld residual stresses by Dong [9]. The results based on the estimation scheme are labeled with circular symbols (in blue) and FEA results using straight line (in red). Note that all residual stress results are compared at component OD surface in Figs. 11 and 12, and all remaining figures. It can be seen that the two sets of results are in a good agreement from weld toe position to a distance of about 2.5 \sqrt{rt} beyond which residual stresses become negligible in both $r/t=10$ (Fig. 11) and $r/t=100$ (Fig. 12). The same can be said for the case with wall thickness of 25 mm (1”) and r/t ratio of 10, shown in Fig. 13.

For thick wall section, two cases of 100 mm (4”) thick with single V joint preparation are presented in Figs. 14 and 15. One is with r/t ratio of 10, and the other is 100. Again, an excellent agreement between shell theory based estimations and FEA results can be observed.

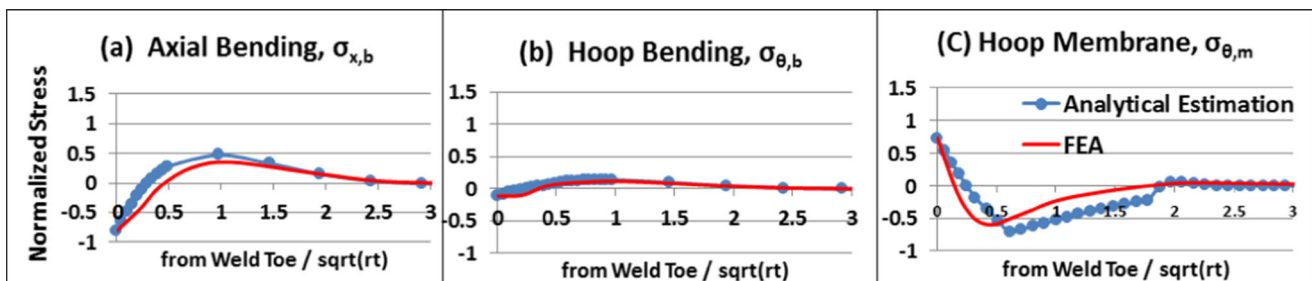


Fig. 11 Shell theory based estimation scheme versus finite element results for single V girth weld, thickness of 6.25 mm (1/4”) and r/t of 10. **a** Axial bending residual stresses, **b** hoop bending residual stresses, and **c** hoop membrane residual stresses

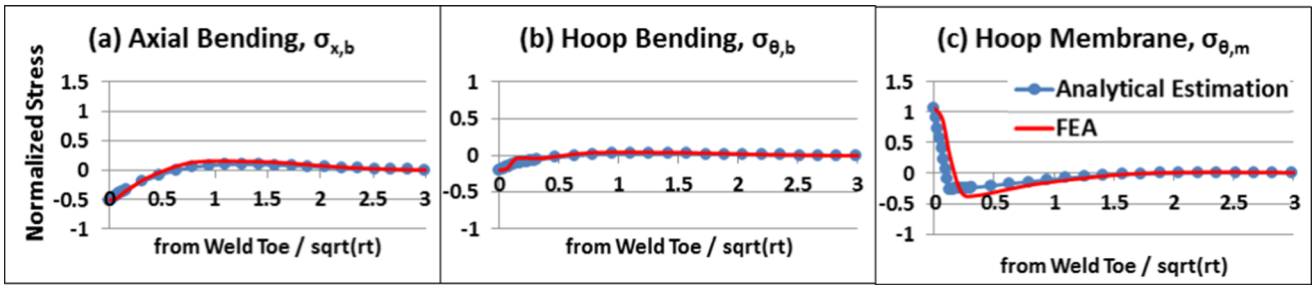


Fig. 12 Shell theory based estimation scheme versus finite element results for single V girth weld, thickness of 6.25 mm (1/4”) and r/t of 100. **a** Axial bending residual stresses, **b** hoop bending residual stresses, and **c** hoop membrane residual stresses

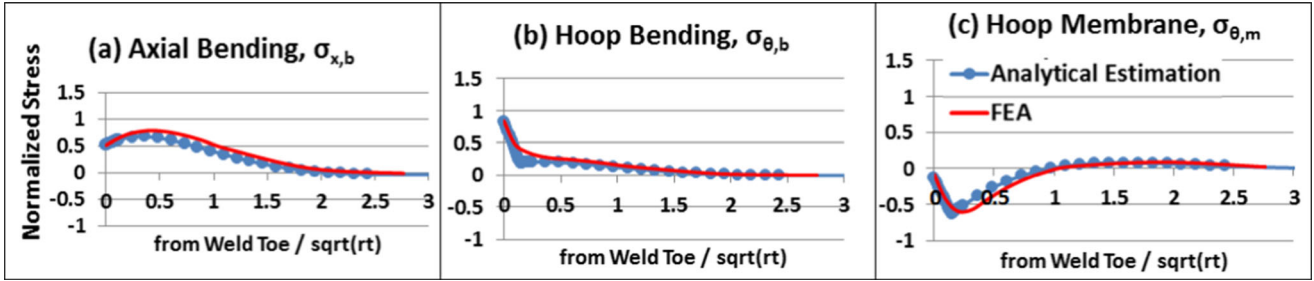


Fig. 13 Shell theory based estimation scheme finite element results for single V girth weld, thickness of 25 mm (1”) and r/t of 10. **a** Axial bending residual stresses, **b** hoop bending residual stresses, and **c** hoop membrane residual stresses

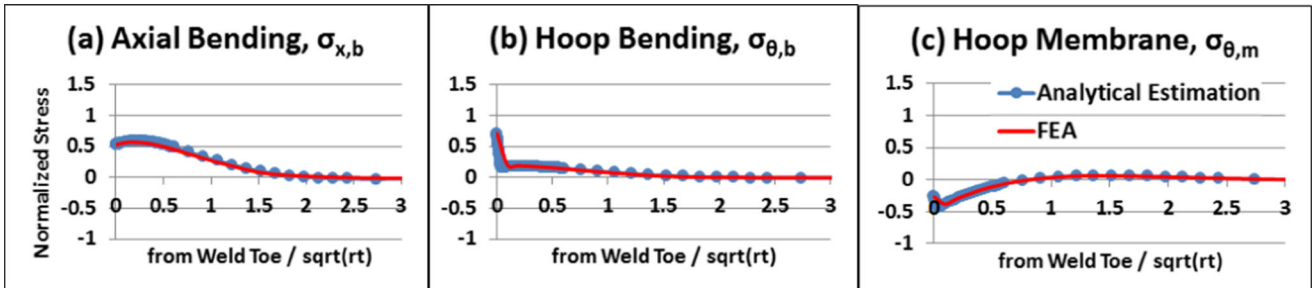


Fig. 14 Shell theory based estimation scheme versus finite element results for single V girth weld, thickness of 100 mm (4”) and r/t of 10. **a** Axial bending residual stresses, **b** hoop bending residual stresses, and **c** hoop membrane residual stresses

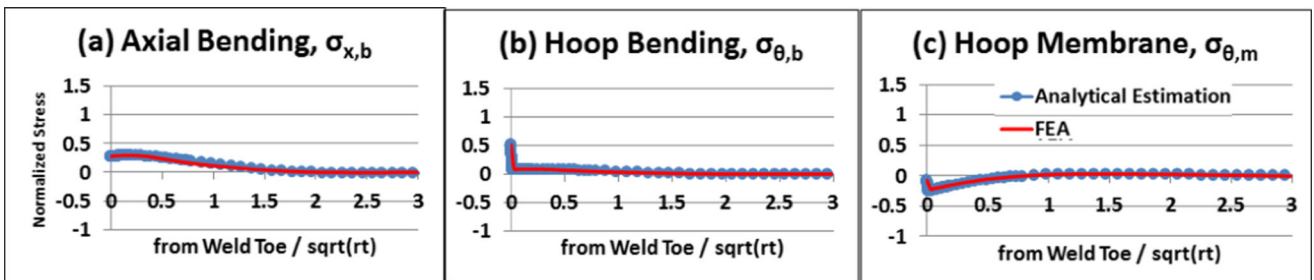


Fig. 15 Shell theory based estimation scheme versus finite element results for single V girth weld, thickness of 100 mm (4”) and r/t of 100. **a** Axial bending residual stresses, **b** hoop bending residual stresses, and **c** hoop membrane residual stresses

6 Application demonstration

In this section, the full-field residual stress estimation scheme presented in this paper will be demonstrated for two girth welded components corresponding to rather different wall thicknesses and r/t ratios. Note that within the weld zone, Section 4 provides the procedure for through-thickness residual stress profile estimation for both weld centerline and weld toe position. Section 5 provides the shell theory based analytical method for residual stress profile estimation for any axial location beyond weld zone.

6.1 Case definitions

A thick section girth weld is considered here for demonstrating how the full-field residual stress profile estimation procedure developed in the previous two sections can be used to establish through-thickness residual stress distributions for both axial and hoop components. All parameters describing geometric, material, and welding procedures are listed in Table 1.

With the information given in Table 1, the derived parameters required by the full-field residual stress profile estimation scheme are summarized in Table 2. Note that the membrane and bending stresses listed in Table 2 are used to compute input parameters to the shell theory based estimation scheme, as summarized in Table 3. The relevant equations used in computing these input parameters are also listed in Table 3 (2nd column) for clarity.

Table 1 Parameters describing two girth welded components

Joint preparation	Single V	
Pipe/weld material	Pipe steel	
Young's modulus E [Gpa]	220.448	
Yield strength S_y [MPa]	558	
Density ρ [Kg/mm ³]	7.84E-6	
Specific heat C_p [J/Kg/°C]	448	
Thickness t [mm]	254 (10")	100 (4")
r/t ratio	10	2
Linear heat input Q [J/mm]	4240	1144
Fusion zone and pass profile	17 layers	11 layers
	79 passes	67 passes
Fusion zone size A_w [mm ²]	37,840	6650
Averaged pass area A_{pass} [mm ²]	490	99
Molten weld deposit size r_w [mm]	12.5	5.6
ΔT_y [°C]	183.4	

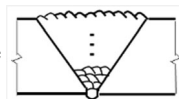


Table 2 Derived parameters based on the procedure presented in Sec. 4

r/t	10	2
$\hat{Q} = Q/A_w$	0.112	0.172
$\sigma_{x,b}^0$	0.55	0.783
$\sigma_{\theta,b}^0$	0.66	0.854
$\sigma_{\theta,m}^0$	-0.278	-0.39
$\sigma_{\theta,m}^{ave}$	0.66	0.429

Table 3 Calculated input parameters to be used by shell model

Parameters	Equation used	$t=254,$ $r/t=10$	$t=100,$ $r/t=2$
Plastic zone boundary d_p [mm]	Eq. (27)	30	20
Plastic zone area A_p [mm ²]	Eq. (25)	53,080	10,714
Shrinkage force F_p [N]	Eq. (17)	19,549,364	2,560,646
Ring force Q_0 [N/mm]	Eq. (17)	3665	5040
Ring moment M_0 [N-mm/mm]	Eq. (19)	3,299,993	751,678
$\Delta\sigma_{\theta,b}$	Eq. (31)	0.495	0.65
$\Delta\sigma_{\theta,m}$	Eq. (32)	0.24	0.426

6.2 Estimated residual stress profile

As given in Section 4, through-thickness residual stress profile for both axial and hoop components can be estimated as:

$$\frac{\sigma(\xi)}{S_y} = \bar{\sigma}_m + \bar{\sigma}_b\xi + \bar{\sigma}_{s.e.}(\xi) \quad 0 \leq x \leq d_p \tag{33}$$

$$\frac{\sigma(\xi)}{S_y} = \bar{\sigma}_m + \bar{\sigma}_b\xi \quad x > d_p$$

where x is measured from weld toe and S_y is material yield strength. ξ is a dimensionless coordinate parameter along through-thickness direction with ID at $\xi=-1$ and OD at $\xi=1$. The self-equilibrating term $\bar{\sigma}_{s.e.}(\xi)$ is given by Eq. (8) in Section 4.

The estimated results at various axial locations are presented in Fig. 16 for wall thickness of 250 mm and $r/t=10$. Note that Sections A-A and B-B are given by the procedure described by Eq. (7) in Section 4. For $x>0$, Eq. (33) (after inserting Eqs. 28 through 32) in conjunction with parameters given in Table 3 provides a continuous estimation of through-thickness residual stress profile as a function of x . For comparison purpose, finite element results obtained for the same girth weld are also plotted in Fig. 16. It can be seen that the full field residual stress estimation scheme is capable of providing satisfactory

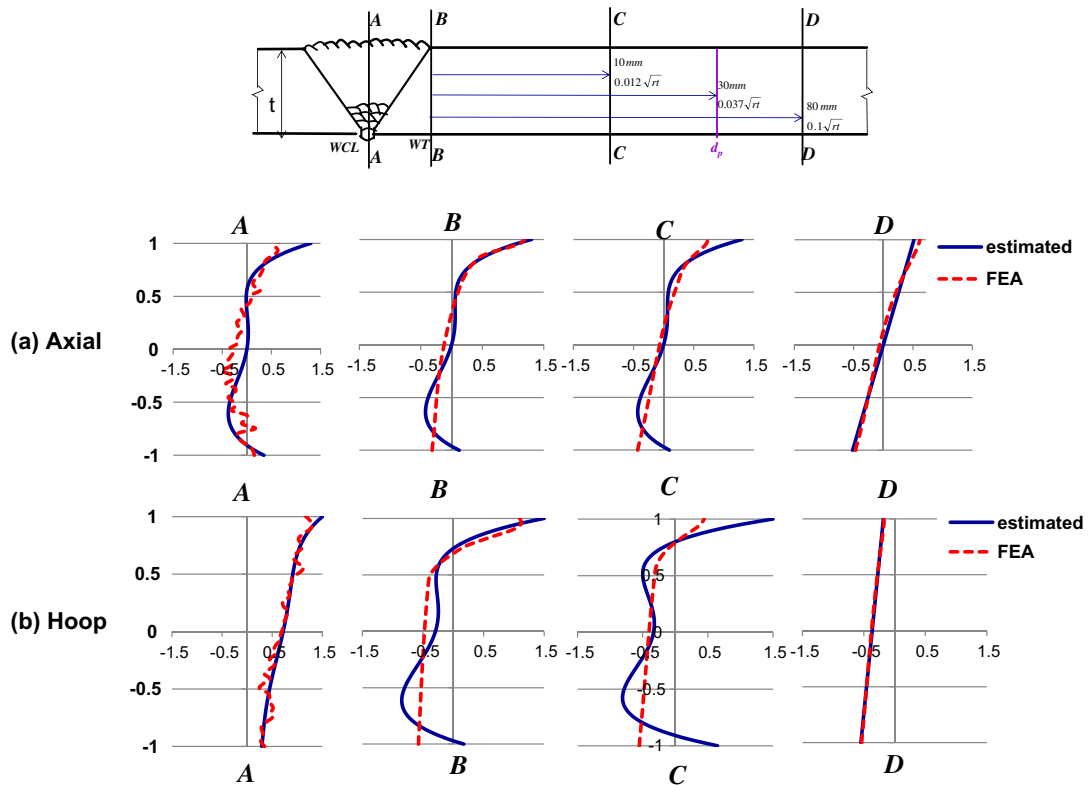


Fig. 16 Single V, $t = 250$ mm (10”), $r/t = 10$: comparison of axial and hoop residual stress profiles between estimated (“estimated”) using Eq. (33) versus finite element results (“FEA”) at different locations. **a** Weld centerline, **b** weld toe, **c** 10 mm away from weld toe, and **d** 80 mm away from weld toe

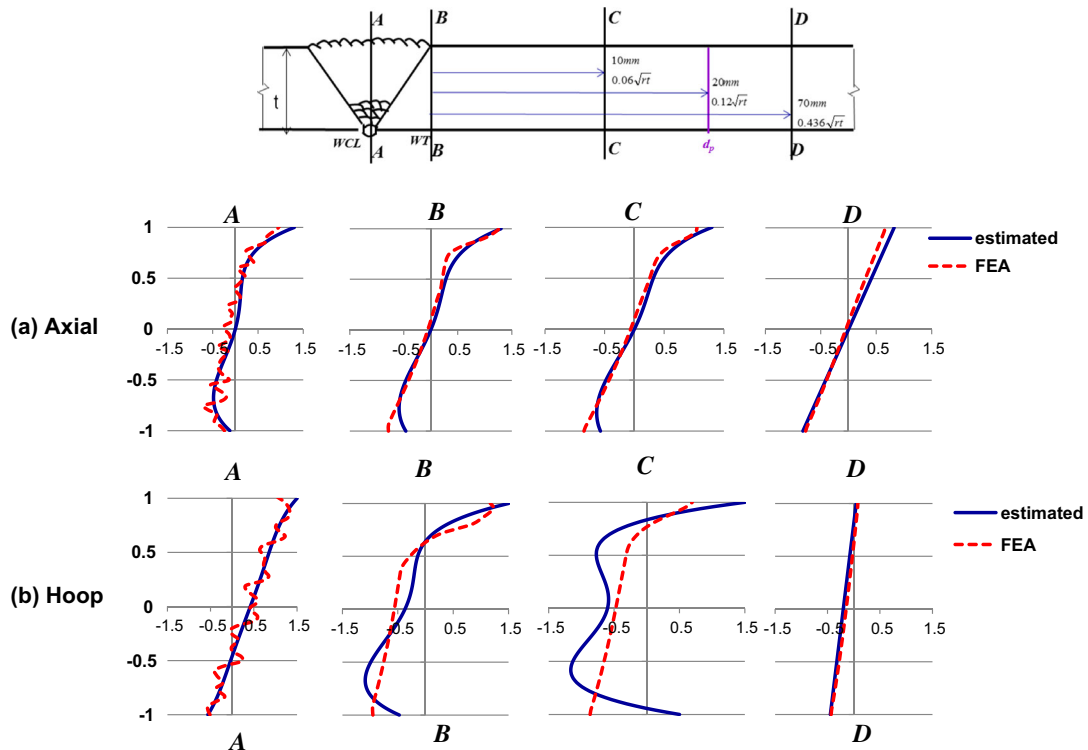


Fig. 17 Single V, $t = 100$ mm (4”), $r/t = 12$, comparison of axial and hoop residual stress profiles between estimated (“estimated”) using Eq. (33) versus finite element results (“FEA”) at different locations. **a** Weld centerline, **b** weld toe, **c** 10 mm away from weld toe, and **d** 80 mm away from weld toe

residual stress profiles for all locations in pipe or vessel girth welds with self-equilibrating stresses somewhat over-estimated to be conservative. A similar comparison can also be seen for the case with wall thickness of 100 mm and $r/t=2$, as shown in Fig. 17. For another extreme r/t ratio, such as $r/t=100$ with $t=100$ mm, Fig. 15 clearly shows that the full-field residual stress estimation scheme also gives satisfactory results.

In addition, comparing with Fig. 15 ($r/t=10$, thickness=100 mm) and Fig. 17, it can be clearly seen that both axial bending and hoop membrane stresses for $r/t=100$ become much less significant (or becoming more self-equilibrating dominated) than those for $r/t=10, 2$, respectively. The proposed estimation scheme is based on parametric analysis results for girth welded components for r/t ratio varying from $r/t=2$ to 100. Note that for pure self-equilibrating residual stress distribution in through-thickness direction, $\bar{\sigma}_m$ and $\bar{\sigma}_b$ in Eq. (33) become drop out. The remaining self-equilibrating component $\bar{\sigma}_{s.e.}$ can then be estimated by Eq. (8) through self-equilibrating conditions given in by Eq. (9) and consistency conditions given in Eqs. (10) and (11).

7 Concluding remarks

Through a large number of parametric analyses of girth welded components with a broad range of radius to thickness ratio (r/t), wall thickness (t), heat input, and joint preparations, two key controlling parameters have been identified, which play a dominant role in determining through-thickness residual stress distributions. These two parameters are as follows:

- (1) Component radius to thickness ratio (r/t), which measures radial bending stiffness that dominates both membrane and bending parts of through-thickness residual stress distributions in axial and hoop directions
- (2) Characteristic heat input parameter (\hat{Q}) which can be directly related to weld shrinkage force in hoop direction and serve as a key driving force for generating bending part of the axial residual stress

With the two parameters, a shell theory based two-part assembly model is introduced as a means of estimating residual stress distributions away from weld region. With this shell-theory based analytical model, a full-field residual stress profile estimation can now be achieved for girth welds in pressure vessels and piping components, not only within weld region, but also at any locations away from weld.

The proposed estimation scheme offers both consistency and well-defined mechanics basis in residual stress profile generation and should be well suited for supporting fracture mechanics based fitness for service assessment for girth welds in pressure vessel and piping components.

Acknowledgments The authors acknowledge the support of this work in part through a grant from Pressure Vessel Research Council (PVRC) at University of New Orleans and a grant from the National Research Foundation of Korea (NRF) Gant funded by the Korea government (MEST) through GCRC-SOP at University of Michigan under Project 2–1: Reliability and Strength Assessment of Core Parts and Material System.

References

1. Dong P, Hong JK. (2002) “Analysis of IIW X/XV RSDP phase I round-robin residual stress results,” IIW Welding In the World, Volume 46, 5–6, pp 24–31
2. BS7910:2013 (2013) Guide to Methods of Assessing the Acceptability of Flaws in Metallic Structures, London: British Standards Institution
3. Procedure R6 Revision 4, (2013) Assessment of the integrity of structures containing defects, British Energy Generation Ltd
4. Api RP (2007) 579-1/ASME FFS-1. American Petroleum Institute, Houston
5. Bouchard PJ (2007) Validated residual stress profiles for fracture assessments of stainless steel pipe girth welds. Int J Press Vessel Pip 84(4):195–222
6. Dong P, Hong JK (2007) On the residual stresses profiles in new API 579/ASME FFS-1 appendix E. Weld World 51:119–127
7. Dong P, Song S, Zhang J, Kim MH (2014) On residual stress prescriptions for fitness for service assessment of pipe girth welds. Int J Press Vessel Pip 123–124:19–29
8. Dong P (2008) Length scale of secondary stresses in fracture and fatigue. Int J Press Vessel Pip 85:128–143
9. Dong P (2007) On the mechanics of residual stresses in girth welds. J Press Vessel Technol 129:345–354
10. Dong P, Hong JK, Bouchard PJ (2005) Analysis of residual stresses at weld repairs. Int J Press Vessel Pip 82:258–269
11. Dong P, Hong JK (2003) Recommendations on residual stresses estimate for fitness-for-service assessment. WRC Bulletin No. 476. Welding Research Council, New York
12. Dong P (2005) Residual stresses and distortions in welded structures: a perspective for engineering applications. Sci Technol Weld Join 10(4):389–298
13. Dong P, Song S, Zhang J (2014) Analysis of residual stress relief mechanisms in post-weld heat treatment. Int J Press Vessel Pip 122: 6–14
14. Song S, Dong P. (2014) Residual stresses in weld repairs and mitigation by design. Proceeding of ASME 2014 OMAE Conference, OMAE2014-24547, San Francisco, California, USA, 8–13
15. Song S, Paradowska AM, Dong P (2014) Investigation of residual stresses distribution in titanium weldments. Mater Sci Forum 777: 171–175
16. Brust FW, Dong P, Zhang JA. (1997) Constitutive Model for Welding Process Simulation Using Finite Element Methods. Adv Comput Eng Sci; 51–56
17. ABAQUS/Standard User’s Manual, version 6.10-EF, Providence, RI, 2011
18. Yaghi AH, Hyde TH, Becker AA, Sun W, Hilson G, Simandjuntak S, Flewitt PEF, Pavier MJ, Smith DJ (2010) A comparison between measured and modeled residual stresses in a circumferentially butt-welded P91 steel pipe. J Press Vessel Technol 132:10
19. Yaghi AH, Hyde TH, Becker AA, Sun W (2007) Numerical simulation of P91 pipe welding including the effects of solid state phase transformation on residual stress. Proc Inst Mech Eng Part L 221: 213–224
20. Dong P, Hong JK (2002) Analysis of IIW X/XV RSDP phase I round-robin residual stress results. Weld World 46:24–31

21. Brickstad B, Josefson BL (1998) A parametric study of residual stresses in multi-pass butt-welded stainless steel pipes. *Int J Press Vessel Pip* 75(1):11–25
22. Yaghi AH, Hyde TH, Becker AA, Sun W, Williams JA (2006) Residual stress simulation in thin and thick-walled stainless steel pipe welds including pipe diameter effects. *Int J Press Vessel Pip* 83:864–874
23. Song S, Dong P, Pei X (2015) A full-field residual stress estimation scheme for fitness-for-service assessment of pipe girth welds: part I: identification of key parameters. *Int J Press Vessel Pip* 126–127:58–70
24. Song S, Dong P, Pei X (2015) A full-field residual stress estimation scheme for fitness-for-service assessment of pipe girth welds: part II—a shell theory based implementation. *Int J Press Vessel Pip* 128: 8–17
25. Song S, Pei X, Dong P. (2015) An analytical interpretation of welding linear heat input for 2D residual stress models. PVP2015-45753. Proceeding of ASME 2015 PVP Conference, Boston, Massachusetts, USA, 19–23
26. Timoshenko S. (1959) *Theory of Plates and Shells*. 2nd Edition. McGraw-Hill, Inc. ISBN 0-07-085820-9
27. Pei X, Song S, Dong P. (2015) An analytical method for estimating welding-induced plastic zone size for residual stress profile development. PVP2015-45750. Proceeding of ASME 2015 PVP Conference, Boston, Massachusetts, USA, July 19–23
28. Song S, Dong P, Zhang J. (2012) A full-field residual stress profiles estimation scheme for pipe girth welds. PVP2012-78560. Proceeding fo ASME 2012 PVP Conference, Toronto, Ontario, Canana, July 15–19